Vacuum 162 (2019) 156–162

Contents lists available at ScienceDirect

Vacuum

journal homepage: www.elsevier.com/locate/vacuum

Analysis of electronic and optical properties of copper iodide (γ-CuI) by TB – mBJ method – A promising optoelectronic material

R. Vettumperumal[a,*], J. Ruby Jemima[b,c], S. Kalyanaraman[c], R. Thangavel[d]

[a] Department of Physics, V.V. College of Engineering, Tisaiyanvilai, India
[b] Department of Physics, St. Johns College, Palayamkottai, India
[c] P.G. and Research Department of Physics, Sri Paramakalyani College, Alwarkurichi, India
[d] Department of Applied Physics, Indian Institute of Technology, Dhanbad, India

ARTICLE INFO

Keywords:
Copper iodide
Density functional theory
TB – mBJ
Optical properties

ABSTRACT

Density functional theory (DFT) calculations using full potential linearized augmented plane wave (FP-LAPW) method as implemented in the Wien2k code have been performed to investigate the structural, electronic and optical properties of copper iodide (γ- CuI) in zinc blende phase. Optical properties have been studied theoretically and various optical constants such as complex dielectric constant, refractive index, reflectance, transmittance, absorption co-efficient, optical conductivity and electron energy loss are discussed with respect to the photon energy. We have also discussed the progresses of the overall results of Tran–Blaha modified Becke–Johnson (TB-mBJ) potential and have been compared to the standard generalized gradient approximation (GGA) method. Exciton binding energy is also calculated and the value is found to be 60 meV. As the absorption coefficient is maximum in the ultra-violet (UV) region for CuI, it is a very good material active in UV region and hence it can be used in optoelectronic device applications.

1. Introduction

A number of wide band gap semiconductors have attracted the attention of researchers due to their applications in semiconducting electronic devices [1–3]. Copper iodide (γ - CuI) has attracted particular interest owing to several factors such as the large band gap with *p* – type conductivity, negative spin orbit [4], unusually large temperature dependence [5], diamagnetic behavior [6], a large ionicity, and different pressure crystallographic phases (cubic, wurtzite, and zinc blend) compared with the III–V and II–VI compounds [7,8]. The electronic properties of this material have been studied for many years [9,10], and their structural behavior and unusual vibrational properties have also been studied [11]. Maurer *et al* [12] had experimentally reported that the electrical conductivity of cuprous iodide varied with the concentration of the absorbed iodine. Furthermore, the structural and electronic properties of γ-CuI have been widely studied theoretically [13–15]. For instance, Wang *et al* [16] have studied the electronic structure and magnetic properties of γ-CuI doped with 3*d* transition metal (TM) atoms using the generalized-gradient approximation (GGA) method. Recently, Pishtshev *et al* [17] have elaborated a theoretical scheme that provides the microscopic basis for realistic understanding of different properties (stability, chemical bonding and electronic) of γ-CuI using the combination of DFT-based computational and group theory methods. It is well known that the local density approximation (LDA) and GGA often underestimate the band gap. To overcome this problem, researchers have developed approximation methods that are used to include orbital dependent effects and/or some of the essential correlation.

However, in principle, one cannot compare the Kohn – Sham (KS) gap with the experimental band gap since it differs from the experimental gap by the neglected derivative discontinuity Δ_{xc} [18,19]. This Δ_{xc} is a significant parameter that needs to be corrected in the case of semiconductors and insulators. There are different schemes available, such as the optimized effective potential (OEP) method [20,21], hybrid functional method as proposed by Heyd, Scuseria, Ernzerhof (HSE) [22,23] and so on to improve the KS band gap. Unfortunately, these schemes are computationally expensive compared to the LDA or GGA. Also, the GW (One-Particle Green Function (G) with Screened Coulomb Interaction (W)) approximation [24] is a many-body perturbation theory, which represents the state of art technique to calculate the quasi particle correction to the band gap of solids. It is computationally very taxing, however the recently proposed Tran–Blaha modified version of the Becke–Johnson potential (TB-mBJ) [25] has proved to be a successful method for calculating the band gaps of semiconductors and

* Corresponding author. V V College of Engineering, Tisaiyanvilai, 627657, India.
E-mail address: vettumperumalphy@gmail.com (R. Vettumperumal).

https://doi.org/10.1016/j.vacuum.2019.01.047
Received 8 December 2018; Received in revised form 27 December 2018; Accepted 27 January 2019
Available online 29 January 2019
0042-207X/ © 2019 Elsevier Ltd. All rights reserved.

insulators. Computationally, it is as economical as the LDA or GGA although its self-consistency cycle converges slower and therefore requires more iteration (a factor of 2–3). The TB-mBJ scheme is rapidly gaining popularity and significant numbers of studies have been carried out reporting improvements in the band gaps [26–35] since 2009.

Moreover the optical properties of CuI thin films and nanoparticles have been studied by experimental methods but they have yet led to definite conclusions [36–38]. Theoretical work has not been reported for the optical properties of CuI from track records. The present work employs structural, electronic and optical properties of CuI using GGA – PBE potential and has also shown progress in their properties by adopting the modified Becke Johnson potential.

2. Computational details

The first principle calculation of zinc blende CuI (space group: *F43m*) structure is performed by solving Kohn – Sham equation using full potential linearized augmented plane wave (FP – LAPW) method which is a part of the DFT as implemented in Wien2k code [39]. The structural, electronic and linear optical properties of CuI structure is calculated using GGA exchange correlation potential proposed by Perdew – Burke – Emzerholf (PBE). Since this method underestimates the energy gap and fares poorly in locating *d* and *f* orbitals the present calculations are performed using modified Becke Johnson (mBJ) potential for obtaining more accurate results.

In this FP-LAPW method, there are no shape approximations to the charge density or potential. Space around the atoms in the unit cell is divided into two regions such as, (*i*) a spherical muffin-tin (MT) around the nuclei in which the radial solutions of the Schrödinger equation and their energy derivatives are used as basic functions, (*ii*) the interstitial region between the muffin-tins, in which the basis set consists of plane waves [40]. The cut-off energy which defines the separation between the core and valence states is set at −6.0 Ry. The atomic position and sphere radii used are (000) and 2.04 *a.u.* for Cu, (1/4 1/4 1/4) and 2.43 *a.u.* for I, respectively. Augmented plane wave (APW) plus local valence orbitals are used with the wave functions, while the potentials and charge densities are expanded in terms of spherical harmonics inside the muffin-tin spheres. Well-converged solutions were obtained with $R_{MT}\,K_{max.} = 7.0$ (where R_{MT} is the smallest muffin-tin radii and K_{max} is the plane wave cut-off) and *k*-point sampling is checked. Self-consistent calculations are considered to converge when the total energy of the system is stable within 0.0001 Ry. The optoelectronic properties of the compound are calculated using a denser mesh of 1000 *k*-points in the irreducible Brillouinzone (IBZ). The DFT method has proven to be one of the most accurate methods for the computation of the electronic structure of solids [41–46].

3. Results and discussions

3.1. Structural properties

The ground state structural properties of CuI are evaluated by performing volume optimization using the Murnaghan's equations of states (EOSs) [47]. The volume optimization curve of CuI is shown in Fig. 1. It is noticed that the bulk modulus value is 43.98 GPa, which indicates the CuI structure has a moderate strength. The calculated elastic constants (C_{ij}) are positive and satisfy the mechanical stability criteria [48]. The bulk modulus (B) value which should also satisfy the criterion $C_{12} < B < C_{11}$ is found to be true in the present case. From the calculated value of Poisson's ratio (0.31), a high ionic contribution in an intra – atomic bonding for this compound is confirmed. According to Pugh's criteria [49], the critical value to separate the ductility and brittleness is 1.75. If $B/G > 1.75$ the material is ductile, otherwise it is brittle. In the present study, the calculated value of B/G ratio is 2.166 and hence we conclude that CuI has a ductile behavior.

The band structure of CuI is presented in Fig. 2. The direct

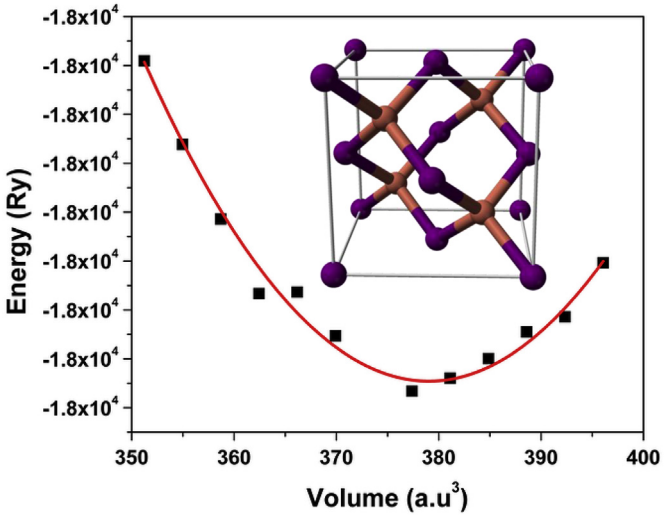

Fig. 1. Structural optimization plot of CuI in zinc blend structure, inset- Unit cell structure of γ-CuI.

fundamental band gap of CuI corresponds to the energy difference of valleys at *Γ* points in the first Brillouin zone. The calculated band gap value of CuI is 1.05 eV for GGA which is much less than the experimental band gap value. The reason being is the insufficient flexible exchange correlation energy and its derivatives. In order to get better estimation of the energy band gap values, the modified Becke – Johnson potential (TB – mBJ) method as proposed by Tran and Blaha [25] has also been employed. Based on this method, the calculated band gap value of CuI is 2.42 eV, which matches with the previously reported theoretical values [50]. However, the difference in band gap value of 0.68 eV may be due to the misleading value of muffin tin radius of the outermost orbitals and the underestimation of bandwidth arising due to the electronic dispersion [51]. The calculated structural parameters are listed in Table 1.

The total density of states (DOS) is an excellent replica of the result found in the band structures. It is in good agreement with the previously calculated theoretical [52,53] and experimental values [54–56]. Total and partial density of states of CuI is presented in Fig. 3, which is generated using 1000 *k*-points in the first Brillouin zone. It shows five distinct peaks VB1, VB2, VB3, and VB4 for valence bands and CB1 for the conduction bands. VB4 is an isolated band which is formed by an atom centered anion *s* valence state. VB3 is *sp*3 like bonding valence state involving largely cation *s* and anion *p* orbitals. VB2 is represented by a core like flat band which consists of the $x^2 - y^2$ and $3z^2 - r^2$ like Cu^+ orbitals and does not participate in the bonds [57]. VB1 is a bonding valence state involving *d* cations and *p* anion orbitals and CB1 is the antibonding counterpart of the VB4 band. From the DOS spectra, we observe that the VB4 – CB1 band gaps are largely homopolar, separating a predominantly Cu 3*d* from Cu 4*s* level one. However, the VB3 – CB1 gap is 8.1 eV which is heteropolar in nature and very similar to the principle gap of ionic solids. This is in agreement with the fact that the CuI is more ionic [58] than the III – V and II – VI compounds.

3.2. Charge density calculation

The bond character of the CuI structure is analyzed by the charge density calculation using contour plot. It gives information about the accumulation of charge around the respective atomic species [59]. Contour plot of the charge density in the CuI structure is displayed in Fig. 4. It shows that a large electronegative difference between Cu and I atoms which causes a charge transfer from Cu to I atoms. It is noticed that the charge density lines are almost spherical in shape in CuI

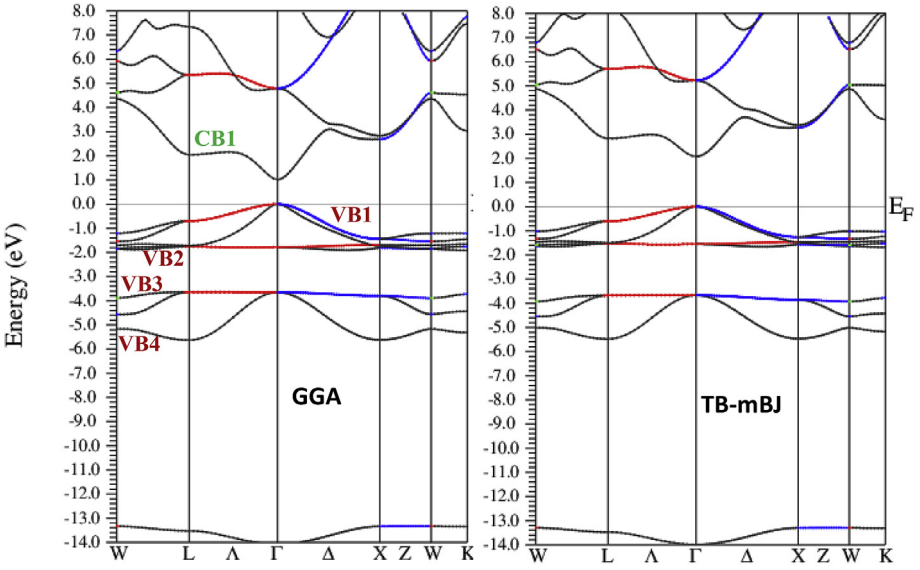

Fig. 2. Band structure plot of CuI with GGA and TB – mBJ potential. The zero energy is E_f.

Table 1
Calculated structural and optical parameters.

Parameters	Present Work		Other Theo. work Ref. [68]	Experiment Ref. [69,70]
	GGA	TB – mBJ		
Lattice Constant (Å)	6.0758	–	6.097	6.054
Band Gap (eV)	1.05	2.42	1.077	3.1
Bulk Modulus (GPa)	43.98	–	58.483	36.6
Young's Modulus (GPa)	52.98	–	–	–
Shear Modulus (GPa)	20.30	–	–	–
Poisson's Ratio	0.31	–	–	–
Lame's Constant	30.45	–	–	–
Compressibility	0.0227	–	–	–
C_{11}	71.04	–	72.39	45.1
C_{22}	30.44	–	33.80	30.7
Dielectric Constant	7.29	6.15	5.695	9.12
Static dielectric constant	6.32	4.95	4.195	–
Absorption co-efficient	4.74×10^7	5.95×10^7	–	–
Urbach Energy (Eu) (meV)	674	769	–	–
Refractive index	2.71	2.44	2.18	2.64
Static refractive index	2.51	2.21	2.048	–
Optical Conductivity (S/cm)	9.09×10^{15}	9.46×10^{15}	–	10.8×10^{13}
Volume Plasmon (meV)	145	133	–	–
Bohr radius(Å)	37.88	31.96	–	–
Exciton binding energy (meV)	56.96	60	–	62

structure which shows the existence of ionic bond between the Cu and I atoms. It is well supported with the results of DOS and structural properties.

3.3. Optical properties

Optical properties are deduced from the dielectric function of the semiconductor which is given by Ref. [60],

$$\varepsilon(\omega) = \varepsilon_r(\omega) + \varepsilon_i(\omega)$$

where, $\varepsilon_r(\omega)$ and $\varepsilon_i(\omega)$ are the real and imaginary parts of the dielectric constant. Eigen values and electron wave functions are the parameters that are necessary to calculate the frequency dependent dielectric functions. It is directly got from the calculation of electronic band structures. The detailed variation of real and imaginary part of dielectric constant of CuI with photon energy is shown in Fig. 5 (a&b).

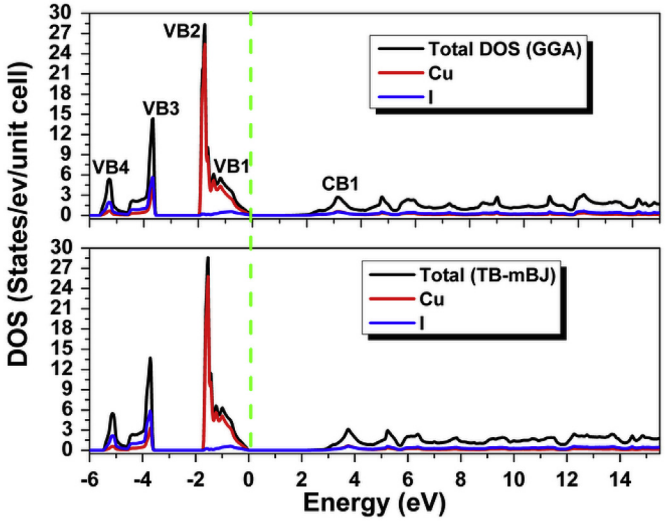

Fig. 3. Total and partial density of states of CuI structure.

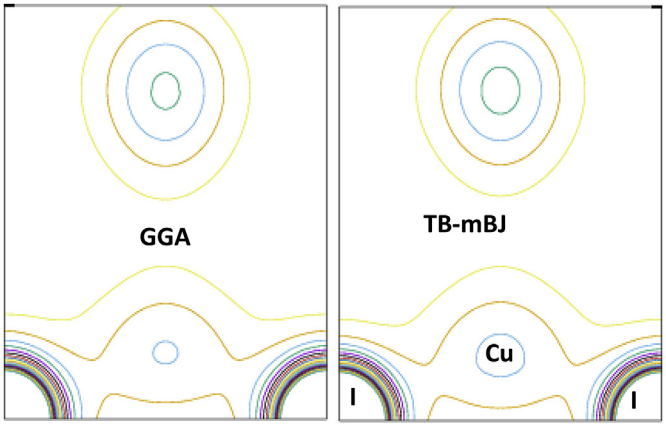

Fig. 4. Charge density contour plot of CuI along (1 1 1) direction.

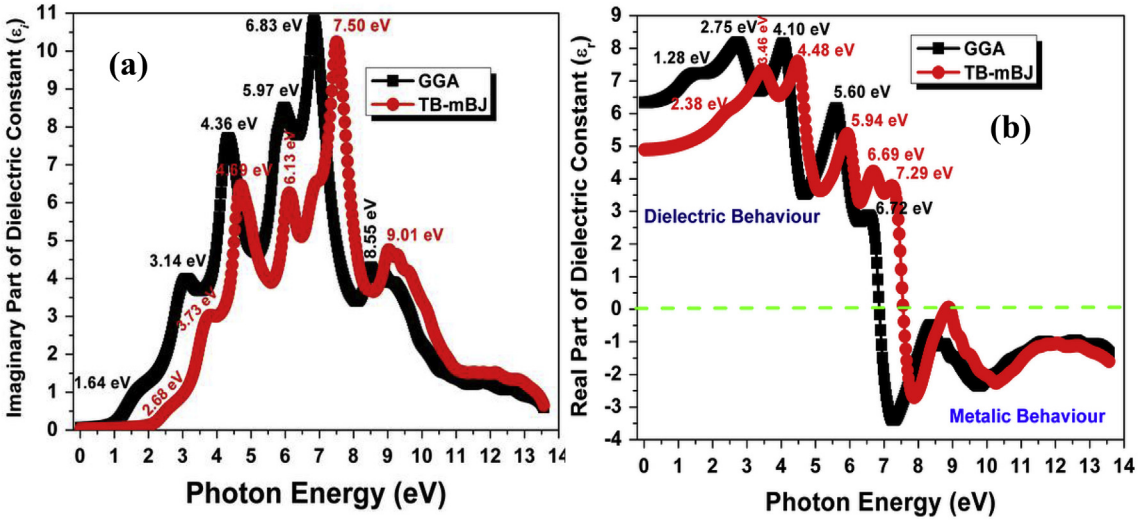

Fig. 5. Plot of complex dielectric constant versus photon energy (a) imaginary part, (b) real part.

Imaginary part of dielectric constant is directly related to the electronic band structures of a material and describes the absorptive behavior. Various interband transitions related peaks are observed at different energies from 3 to 9 eV. These observed peaks are shifted towards the higher energy side in the TB – mBJ method calculations. The maximum intensity of peak is observed at 6.80 eV for PBE and 7.50 eV TB – mBJ method. So, it can also be used as a filter for various energies in the ultra – violet region.

The real part of a dielectric constant can be extracted from its imaginary part using Kramers – Kronig relation with the help of which one can compute various optical constants such as transmittance, reflectance, absorption co-efficient, refractive index and optical conductivity. It is used to characterize the propagation of electromagnetic wave through the material [61]. The calculated real part of dielectric constant is presented in Fig. 5 (b). It shows that the first peak is observed at 1.28 eV for GGA and 2.42 eV for TB – mBJ method. This is related to the excitation of electron from occupied valence band to unoccupied conduction band at Γ point. From the result of the real part of dielectric constant, we find that CuI shows the dielectric behavior ($\varepsilon_r(\omega) > 0$) up to the photon energy around 6.72 eV for GGA and 7.29 eV for TB – mBJ method, while metallic behavior is observed ($\varepsilon_r(\omega) < 0$) above this energy range. Zero energy limit of the real part of dielectric constant gives the value of static dielectric constant ($\varepsilon_r(0)$). The calculated value of $\varepsilon_r(0)$ is 6.32 for PBE method and 4.95 for TB – mBJ. The high value of $\varepsilon_r(0)$ suggests that the CuI has high refractive index and optical density. Various interband transition related peaks in the real and imaginary part of the dielectric constant are shifted towards the higher energy side which is noticed by the TB – mBJ calculation. It is due to the dielectric response of CuI structure.

The relationship between the electric and magnetic fields in a material is described by the complex dielectric constant. Imaginary part of the dielectric constant is directly related to the resistivity, while the real part reveals that the material has a capacitive or inductive optical response. The ratio between these two corresponds to the phase lag between electric and magnetic fields. It is given by Ref. [62],

$$\theta = tan\left(\varepsilon_i/\varepsilon_r\right)$$

The positive (intrinsically capacitive (current leads voltage) optical response) and negative (inductive (voltage leads current) optical response) phase shift of the materials is calculated from the real part of the dielectric constant. Phase shift versus photon energy of CuI is shown in Fig. 6. Capacitive optical response of CuI is observed in the energy range below 4.4 eV for GGA method. Improved capacitive optical response of CuI is observed in the energy range 6.2 eV by the TB – mBJ

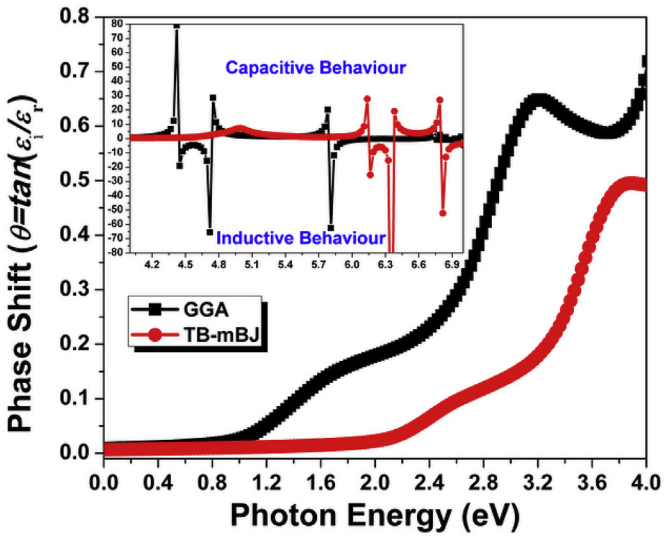

Fig. 6. Phase shift versus photon energy of CuI.

method when compared to the GGA method. Above this energy range there is mixed (capacitive and inductive) optical response, which is shown in inset Fig. 6. From these results, we infer that the CuI structure could be used as a supercapacitor for energy storage applications.

Transmittance and reflectance spectra of CuI structure are calculated by GGA and TB – mBJ correlation potential method and it is displayed in Fig. 7. It is noteworthy that the GGA calculation shows the maximum transmittance is around 65% and reflectance 35% in the visible region. Both transmittance and reflectance varied randomly in the UV region. In the visible region, transmittance and reflectance performances are improved by the TB – mBJ correlation potential method which is 70% and 30%. That categorically explains why the interband transition related peaks are absent in this region. Absorption co-efficient spectra of CuI is shown in Fig. 8. The magnitude of the absorption coefficient increases linearly with increasing of photon energy in the visible region. Band gap related absorption peak and its corresponding absorption co-efficient value are 4.76×10^7 for GGA method and 5.95×10^7 for TB – mBJ method. The maximum intensity absorption coefficient peak (6.79×10^7) is observed at 4.42 eV for TB – mBJ method. From this result, we infer that the CuI structure finds immense scope in the application of optoelectronic devices like UV detector. The interband energy is calculated from the inverse of the

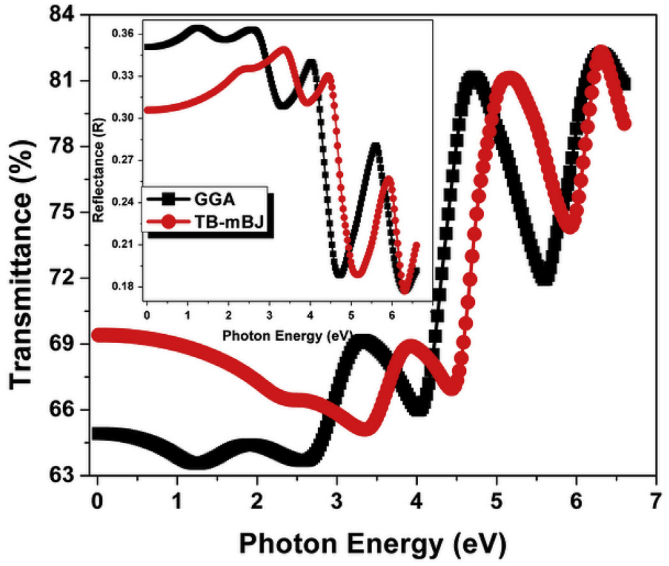

Fig. 7. Transmittance and reflectance (inset) of CuI with GGA and TB – mBJ potential.

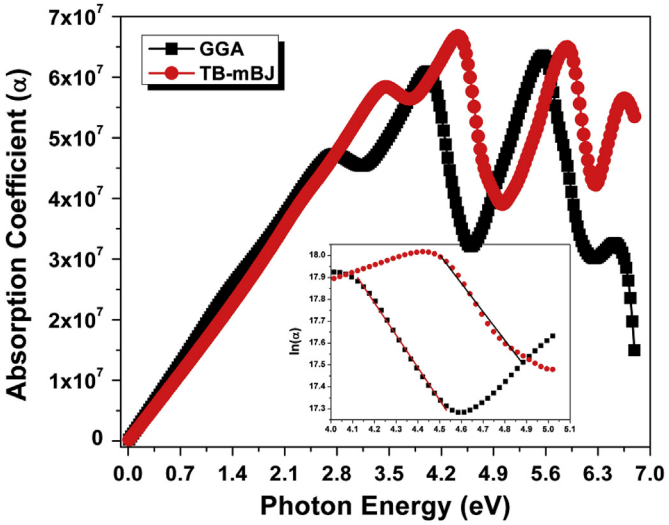

Fig. 8. Absorption co-efficient of CuI, inset: photon energy versus *ln(α)*.

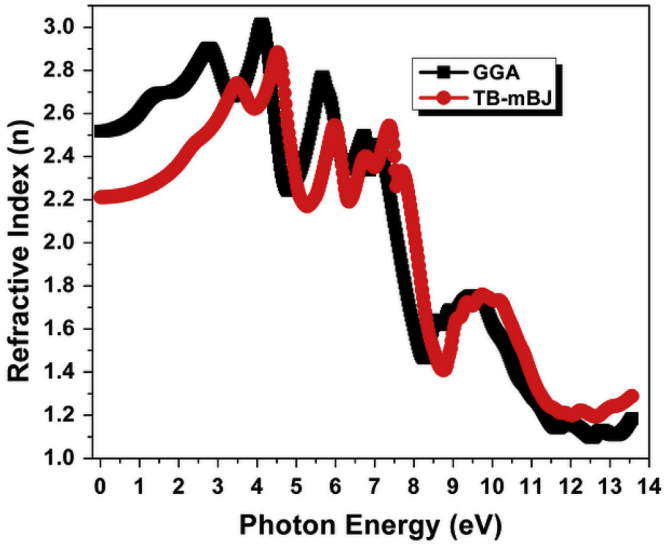

Fig. 9. Refractive index versus photon energy of CuI with GGA and Tb – mBJ potential.

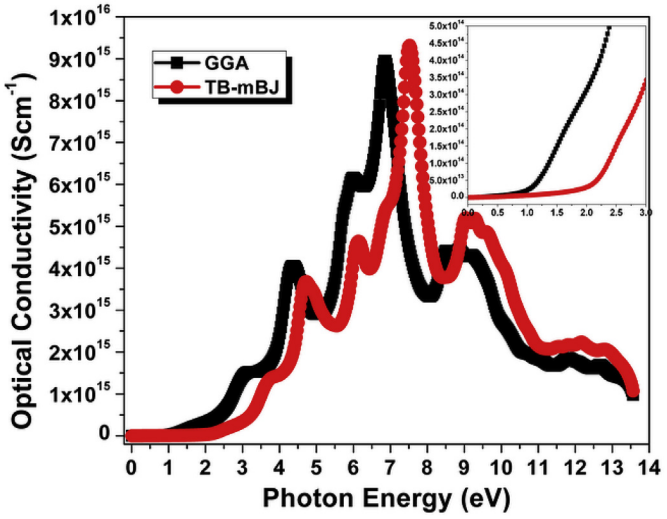

Fig. 10. Optical conductivity of CuI with respect to photon energy.

slope value of linear fit ($ln(\alpha)$ versus photon energy graph), which is shown in the inset of Fig. 8. The calculated interband energy values are 674 meV for GGA and 769 meV for TB – mBJ potentials.

Knowledge of refractive index of a material is an important parameter for its accurate modeling and possible device applications. The calculated refractive index of CuI structure is shown in Fig. 9. This figure reveals that the refractive index increases with the increase of photon energy for GGA and TB – mBJ method. It reaches maximum at 4.11 eV for GGA and 4.54 eV for TB – mBJ method and decreases with the further increase of photon energy. It is due to the interaction of more electrons with photons in this region. It has a tendency to increase gradually in the lower energy region which confirms the optically anisotropic nature of CuI structure. The observed refractive index values in the band gap region are 2.71 for PBE and 2.47 for TB – mBJ methods. It compares favorably with the experimental values. The high value of refractive index is due to the high value of electron density. Static refractive index of CuI is found from the zero-photon energy of refractive index and the value is 2.51 for PBE and 2.21 for TB – mBJ method. Hence, the calculated refractive and static refractive index values are higher than the refractive index of glass (1.5). Hence, we conclude that CuI can be used in antireflection coating applications.

Optical conductivity of CuI is presented in Fig. 10. It starts from 1 eV for GGA and 2 eV for TB – mBJ method which is shown in the inset of Fig. 10. It increases rapidly above this energy due to high density of electrons which augment well with the refractive index results. Further, several peaks are observed corresponding to the bulk plasmon excitations which are caused by the crossover of electrons from valence band to the conduction band. The main peak is situated at 6.84 eV for PBE and 7.53 eV for TB – mBJ method and it corresponds to the optical conductive value of the order of 10^{15}. From this result, we infer that the CuI can be used as photoconductor in the UV region.

Electron energy loss is a valuable tool for investigation of various aspects of materials. It has the advantage of covering the complete energy range including non-scattered and elastically scattered electrons. Primarily, the energy loss is due to complicated mixture of single electrons and collective excitations (plasmon) in the intermediate energy range (typically 1–50 eV) [63]. However, intraband transition arises due to the single electron excitations while interband transition is due to the plasmon. Here, we observe that interband transition is confirmed from the result of complex dielectric functions. The energy loss spectrum is also related to the energy loss of fast electron traversing

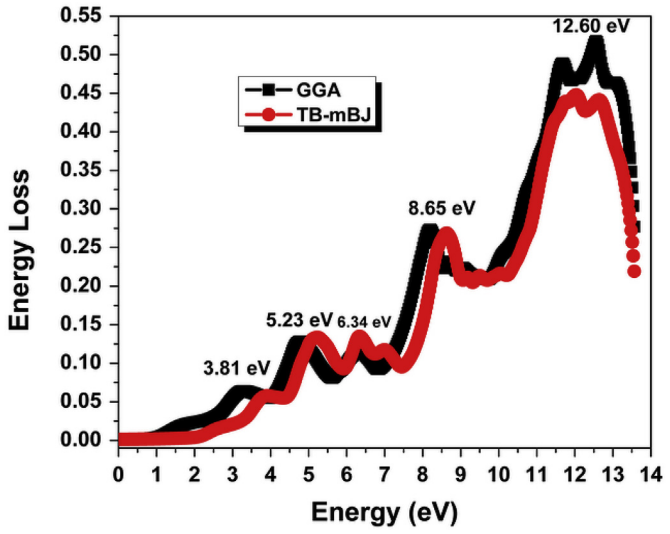

Fig. 11. Energy loos spectra of CuI in zinc blend phase.

in the material and is usually large at the plasma energy [64].

The energy loss spectrum is shown in Fig. 11 and it shows five distinct peaks at 3.81, 5.23, 6.34, 8.65 and 12.60 eV respectively. The most dominant peak (Plasmon peak) in the energy loss spectrum is observed and located at 12.60 eV. It is responsible for the rapid decrease of reflectance confirming the change in reflectance with photon energy as discussed previously. The scattering probability for volume loss is directly connected to the energy loss function. The calculated energy of the volume Plasmon is inversely proportional to the maximum energy of the imaginary part of dielectric constant. The calculated value of the energy of the volume plasmon is 145 meV for GGA and 133 meV for TB – mBJ method. From this result, we infer that the energy loss gets reduced by the TB – mBJ method calculations. The formulas used to calculate the structural and optical parameters are listed in supplementary file.

3.4. Exciton binding energy

The exciton binding energy (EBE) of CuI is calculated using the hydrogenic model [65]. From the parameters, exciton Bohr radius (a^*) and exciton binding energy (E_b) are given by

$$a^* = \frac{m}{m^*}\varepsilon a_0$$

$$E_b = \frac{a^2}{\varepsilon a^*} = \frac{e^2 a_0}{(m^*/m)(a^*)^2}$$

Where, 'm' and 'm^*' are the electron effective and reduced masses ($m_e = 0.33m_0$, $m_h = 1.4m_0$ and $\mu = 0.27m_0$) [66], 'a_o' is the Bohr radius for the hydrogen atom, 'e' is the electron charge and 'ε' is the dielectric constant. The calculated Bohr radius value is 37.88 Å for GGA and 31.96 Å for TB – mBJ method, while the exciton binding energy is 56.96 meV for GGA and 60 meV for TB – mBJ method. The increases of exciton binding energy lead to the increase of electron-hole Coulomb interaction which ultimately decreases the charge density [67]. It is very essential for exciton-based device applications.

4. Conclusions

The structural, electronic and optical properties of CuI are studied using TB – mBJ potential a part of the FPLAPW method. Ductile behavior of CuI is observed from the Pugh's ratio value and direct band gap is observed from the results of band structure and density of states in the first Brillouin zone. Ionic bond behavior between Cu and I is confirmed from the Poisson's ratio values and charge density calculations. Various interband transitions related peaks are observed from the complex dielectric function. The capacitive optical response of CuI is observed up to 6.2 eV from the phase lag between electric magnetic fields. Hence, it can be used as a supercapacitor for energy storage applications. The magnitude of absorption co-efficient is found to be in the order of 10^7 in the UV region and it corresponds to optical conductivity value of the order of 10^{15}. The calculated refractive index (2.47) and static refractive index (2.27) values are higher than the glass refractive index (1.5). Hence, CuI can be used in antireflection coating applications. A rapid decrease in the value of reflectance turns the Plasmon related peak to appear in the energy loss spectrum at 12.60 eV. All the results of calculated parameters by TB – mBJ potential are comparable with GGA however couldn't exactly matches with the experimental results owing to the underestimation of bandwidth. From these, we infer that CuI finds application in ultra-violet photodetectors.

Acknowledgement

We the authors are indebted to the management of Sri Paramakalyani College, Alwarkurichi, Indian Institute of Technology, Dhanbad and V V College of Engineering, Tisaiyanvilai for the facilities provided to complete this work.

Appendix A. Supplementary data

Supplementary data to this article can be found online at https://doi.org/10.1016/j.vacuum.2019.01.047.

References

[1] Y. Gai, J. Li, S.S. Li, J.B. Xia, S.H. Wei, Phys. Rev. Lett. 102 (2009) 036402.
[2] Q. Zhang, C.S. Dandeneau, X. Zhou, G. Cao, Adv. Mater. 21 (2009) 4087.
[3] H. Peng, H.J. Xiang, S.H. Wei, S.S. Li, J.B. Xia, J. Li, Phys. Rev. Lett. 102 (2009) 017201.
[4] M. Cardona, Phys. Rev. 129 (1963) 69.
[5] S.F. Lin, W.E. Spieer, R.S. Baver, Phys. Rev. B 14 (1976) 4551.
[6] C.W. Chu, A.P. Ruskov, S. Huang, S. Early, T.H. Geballe, C.Y. Huang, Phys. Rev. B 18 (1978) 2116.
[7] S. Hull, D.A. Keen, Phys. Rev. B 50 (1994) 5868.
[8] M. Yashima, Q. Xu, A. Yoshiasa, S. Wada, J. Mater. Chem. 16 (2006) 4393.
[9] A. Blacha, N.E. Christensen, M. Cardona, Phys. Rev. B 33 (1986) 2413.
[10] A. Blacha, H. Presting, M. Cardona, Phys. Status Solidi B 126 (1984) 11.
[11] J.W. Kremer, K.H. Weyrich, Phys. Rev. B 40 (1989) 9900.
[12] R. Maurer, J. Chem. Phys. 13 (1945) 321.
[13] B. Amrani, T. Benmessabih, M. Tahiri, I. Chiboub, S. Hiadsi, F. Hamdache, Physica B 381 (2006) 179.
[14] H. Hernandez-Cocoletzi, G. Cocoletzi, J.F. Rivas-Silva, A. Flores, N. Takeuchi, J. Nano Res. 5 (2009) 25 2009.
[15] Y. Ma, J. Tse, D. Klug, Phys. Rev. B 69 (2004) 064102.
[16] J. Wang, J. Li, S.-S. Li, J. Appl. Phys. 108 (2010) 043713.
[17] A. Pishtshev, S. Zh. Karazhanov, J. Chem. Phys. 146 (2017) 064706.
[18] M. Gruning, A. Marini, A. Rubio, J. Chem. Phys. 124 (2006) 154108.
[19] M. Gruning, A. Marini, A. Rubio, Phys. Rev. B 74 (2006) 161103 (R).
[20] J. Heyd, G.E. Scuseria, M. Ernzerhof, J. Chem. Phys. 118 (2003) 8207.
[21] J. Heyd, J.E. Peralta, G.E. Scuseria, R.L. Martin, J. Chem. Phys. 123 (2006) 174101.
[22] W.G. Aulbur, L. Jonsson, J.W. Wilkins, Solid State Phys. 54 (2000) 1.
[23] F. Tran, P. Blaha, Phys. Rev. Lett. 102 (2009) 226401.
[24] G. Barcaro, I.O. Thomas, A. Fortunelli, J. Chem. Phys. 132 (2010) 124703.
[25] W. Feng, D. Xiao, Y. Zhang, Y. Yao, Phys. Rev. B 82 (2010) 235121.
[26] Y.-S. Kim, M. Marsman, G. Kresse, F. Tran, P. Blaha, Phys. Rev. B 82 (2010) 205212.
[27] D.J. Singh, S.S.A. Seo, H.N. Lee, Phys. Rev. B 82 (2010) 180103.
[28] D.J. Singh, Phys. Rev. B 82 (2010) 205102.
[29] M. Catti, Phys. Rev. B 72 (2005) 064105.
[30] S. Hull, D.A. Keen, Phys. Rev. B 59 (1999) 750.
[31] D.J. Singh, Phys. Rev. B 82 (2010) 155145.
[32] S. Gong, B.-G. Liu, Phys. Lett. A 375 (2011) 1477.
[33] N.W. Johnson, J.A. McLeod, A. Moewes, J. Phys. Condens. Matter 23 (2011) 445501.
[34] H. Dixit, N. Tandon, S. Cottenier, R. Saniz, D. Lamoen, B. Partoens, V.V. Speybroeck, M. Waroquier, New J. Phys. 13 (2011) 063002.
[35] D. Koller, F. Tran, P. Blaha, Phys. Rev. B 83 (2011) 195134.
[36] M.N. Amalina, Y. Azilawati, N.A. Rasheid, M. Rusop, Proc. Eng. 56 (2013) 731.
[37] Y. Ma, M. Gu, S. Huang, X. Liu, B. Liu, C. Ni, Mater. Lett. 100 (2013) 166.
[38] H.R. Humud, S.J. Kadhem, D.M. Khudhair, J. Chem. Phar. Res. 9 (1) (2017) 31.
[39] P. Blaha, K. Schwarz, G.K.H. Madsen, D. Kvasnicka, J. Luitz, K. Schwarz (Ed.), WIEN2K: an Augmented Plane Wave Plus Local Orbitals Program for Calculating

Crystal Properties, Vienna Technological University, Vienna, Austria, 2001.
[40] K.E. Babu, N. Murali, K.V. Babu, P.T. Shibeshi, V. Veeraiah, Acta Phys. Pol. A 125 (2014) 1179.
[41] A.H. Reshak, Phys. Chem. Chem. Phys. 16 (2014) 10558.
[42] G.E. Davydyuk, O.Y. Khyzhun, A.H. Reshak, H. Kamarudin, G.L. Myronchuk, S.P. Danylchuk, A.O. Fedorchuk, L.V. Piskach, M.Yu. Mozolyuk, O.V. Parasyuk, Phys. Chem. Chem. Phys. 15 (2013) 6965.
[43] A.H. Reshak, Y.M. Kogut, A.O. Fedorchuk, O.V. Zamuruyeva, G.L. Myronchuk, O.V. Parasyuk, H. Kamarudin, S. Auluck, K.J. Plucinski, J. Bila, Phys. Chem. Chem. Phys. 15 (2013) 18979.
[44] A.H. Reshak, D. Stys, S. Auluck, I.V. Kityk, Phys. Chem. Chem. Phys. 13 (2011) 2945.
[45] A.H. Reshak, RSC Adv. 4 (2014) 39565.
[46] A.H. Reshak, RSC Adv. 4 (2014) 63137.
[47] F.D. Murnagham, Proc. Natl. Acad. Sci 30 (1944) 244.
[48] G. Grimvall, Thermophysical Properties of Materials, Elsevier, Amsterdam, 1999 Enlarged and Revised edition, North Holland.
[49] S.F. Pugh, Philos. Mag. 45 (1954) 823.
[50] A.J. Freeman, C.S. Wang, J. Jarlborg, M. Weinert, F. Wagner, C.W. Chu, J. Quant. Chem. 13 (1979) 445.
[51] D. Waroquiers, A. Lherbier, A. Miglio, M. Stankovski, S. Ponce, M.J.T. Oliveira, M. Giantomassi, G.-M. Rignanese, X. Gonze, Phys. Rev. B 87 (2013) 075121.
[52] S.Y. Ren, R.E. Allen, J.D. Dow, I. Lefkwitz, Phys. Rev. B 25 (1982) 2.
[53] S. Kim, R.S. Williams, Phys. Rev. B 35 (1987) 6661.
[54] A. Goldmann, J. Tejeda, N.J. Shyevchik, M. Cardona, Phys. Rev. B 10 (1974) 4388.
[55] S. Kono, T. Ishii, T. Sagawa, T. Kobayasi, Phys. Rev. B 8 (1973) 795.
[56] S. Lewonczuk, J. Ringeissen, E. Beaurepaire, M.A. Khan, Phys. Rev. B 49 (1994) 2344.
[57] M. Ferhat, A. Zaoui, M. Certier, J.P. Dufour, B. Khelif, Mater. Sci. Eng. B 39 (1996) 95.
[58] J.C. Phillips, Rev. Mod. Phys. 42 (1970) 317.
[59] A.S. Mohammadi, S.M. Baizaee, H. Salehi, World Appl. Sci. J. 14 (10) (2011) 1530.
[60] M. Rashid, F. Hussain, M. Imran, S.A. Ahmad, N.A. Noor, M.U. Sohaib, S.M. Alay-e-Abbas, Chin. Phys. B 22 (2013) 087301.
[61] V.V. Atuchin, B.G. Bazarov, T.A. Gavrilova, V.G. Grossman, M.S. Molokeev, Z.G. Bazarova, J. Alloy. Comp. 515 (2012) 119.
[62] https://www.quora.com/OpticsWhat.is.the.meaning.of.the.maginary.part.of.the.complex.Relative.permittivity.
[63] H. Salehi, H. Tolabinejad, Optic Photon. J. 1 (2011) 75.
[64] T. Ben Nasr, H.B. Abdallah, R. Bennaceur, Physica B 405 (2010) 3427.
[65] M. Dvorak, W. Su-Huai, Z. Wu, Phys. Rev. Lett. 110 (2013) 169904.
[66] M. Veta, H. Kanzaki, K. Kobayashi, Y. Toyozawa, E. Hanamura, Excitonic Processes in Solids, Springer-Verlag Berlin Heidelberg, Tokyo, Japan, 1986, p. 135.
[67] J.J. Kim, S.H. Park, H.M. Kim, J. Kor. Phys. Soc. 43 (2003) 149.
[68] B. Amrania, T. Benmessabih, M. Tahiri, I. Chiboub, S. Hiadsi, F. Hamdache, Physica B 381 (2006) 179.
[69] S. Hull, D. Keen, Phys. Rev. B 50 (1994) 5868.
[70] B.N. Ezealigo, A.C. Nwanya, A. Simo, R.U. Osuji, R. Bucher, M. Maaza, F.I. Ezema, Arab. J. Chem., https://doi.org/10.1016/j.arabjc.2017.01.008.